

**Rethinking the susceptibility-based strategy for marine cloud brightening climate intervention:
experiment with CESM2 and its implications**

Chih-Chieh Chen¹, Jadwiga H. Richter¹, Walker R. Lee¹, Douglas G. MacMartin², Ben Kravitz^{3,4}

¹Climate and Global Dynamics Division, NSF National Center for Atmospheric Research, Boulder, CO

²Cornell University

³Department of Earth and Atmospheric Sciences, Indiana University, Bloomington, IN

⁴Atmospheric Sciences and Global Change Division, Pacific Northwest National Laboratory, Richland,
WA

Key Points:

- We explore the idea of deploying marine cloud brightening over broader regions with low susceptibility to cloud seeding
- This approach induces fairly uniform cooling over the globe unlike marine cloud brightening that targets the most susceptible regions
- This new seeding strategy has fewer climatic side effects and does not trigger a La Nina-like response

Plain Language Summary:

Most previous marine cloud brightening simulations have focused on the regions more likely to induce strong cooling. A common response in these simulations across different climate models is a La Nina-like sea surface temperature pattern which could disrupt the El Nino Southern Oscillation. We explored simulations in which marine cloud brightening is deployed over the least susceptible regions rather than the most susceptible. This new seeding strategy cools the globe more evenly and no longer triggers a La Nina-like response.

Corresponding author: C.-C.Chen, cchen@ucar.edu

Abstract

Previous modeling studies indicate that even though marine cloud brightening under a susceptibility-based strategy is effective in reducing the global average surface temperature, it triggers a La Niña-like sea-surface temperature response with cooling mostly confined within lower latitudes. Here we explore a different cloud seeding strategy involving seeding of regions with low susceptibility. Simulations with the Community Earth System Model, version 2 (CESM2) reveal that because the regional forcing is weaker and more widespread, cooling is more evenly distributed over the globe. This new strategy also does not result in the La Niña-like state seen in the other strategies.

1. Introduction

Carbon emission reduction to mitigate anthropogenic global warming is proceeding slower than is necessary to prevent dangerous anthropogenic interference in the climate system [Friedlingstein et al., 2023]. As such, more attention has been drawn toward research on climate interventions in recent years. Solar climate intervention, one class of climate interventions, aims at enhancing the Earth's albedo and hence increases the reflection of incoming solar radiation. Two proposals for solar climate interventions more widely simulated by climate models are stratospheric aerosol injection (SAI) and marine cloud brightening (MCB). Through climate model simulations, both have been demonstrated to be effective in reducing the global average surface temperature. Nevertheless, the regional climate response under these two climate interventions appears to be significantly different. For SAI [Tilmes et al., 2018; MacMartin et al., 2017; MacMartin et al., 2019; MacMartin et al., 2022; Richter et al., 2022], the injected aerosols become widespread due to the transport processes through atmospheric circulations and thus the induced cooling in general is much more evenly distributed over the globe. With MCB [Rasch et al., 2009; Jones et al., 2009; Hill and Ming, 2012; Hirasawa et al., 2023; Haywood et al., 2023] a global reduction of temperature can also be achieved, however the induced cooling is much more localized around regions where MCB is deployed.

To date, most MCB simulations have assumed deployment of cloud seeding over regions more likely to induce strong cooling. Latham et al. [2008] and Rasch et al. [2009] described a methodology in which regions most susceptible to cloud seeding were first identified and MCB deployment was then prioritized solely based on susceptibility. In other MCB studies [Jones et al., 2009; Hill and Ming, 2012; Hirasawa et al., 2023; Haywood et al., 2023], deployment of cloud seeding was frequently assumed to be over the stratocumulus regions, e.g. the Southeast Pacific, Northeast Pacific, and Southeast Atlantic. With the cloud decks constantly present over

these regions, deployment of MCB is likely to induce strong cooling. Indeed, both strategies have been demonstrated to be viable but the induced cooling was mainly confined to lower latitudes. Furthermore, they tend to trigger a La Nina-like sea surface temperature pattern. This is worrisome as it could disrupt the El Nino Southern Oscillation (ENSO). These attributes could be problematic outcomes for MCB climate intervention.

In this study, we explore cloud seeding strategies over a broader area extent with low susceptibility to cloud seeding. This will exert a weaker, but more globally uniform, forcing on the climate system which might eliminate the undesirable outcomes commonly found in previous MCB simulations.

2. Model description

We use the Community Earth System Model version 2 (CESM2) [Danabasoglu et al., 2020] for all simulations in this study. This version was employed for the Coupled Model Intercomparison Project Phase 6 (CMIP6) [Eyring et al., 2016] in which CESM2 was shown to perform very well in simulating large-scale circulations and tropospheric climate over the historical time period among CMIP6 models [Simpson et al., 2020; Duviver et al., 2020; Coburn and Prunor, 2021].

CESM2 is a fully coupled Earth system model with prognostic atmosphere, land, ocean, sea-ice, and land-ice components. The Community Atmosphere Model version 6 (CAM6) is utilized as the atmosphere component of CESM2, which uses a finite volume dynamical core with a $1.25^\circ \times 0.9^\circ$ longitude-latitude mesh and 32 vertical levels with the model top at around 40 km. CAM6 uses the Zhang and McFarlane [1995] scheme for simulating deep convection, the Cloud Layers Unified By Binormals (CLUBB) [Golaz et al., 2002; Larson, 2017] for shallow convection, boundary layer, and an updated version of Morrison-Gottelman microphysics scheme (MG2) [Gottelman and Morrison, 2015] for representing stratiform clouds and precipitation processes.

The Parallel Ocean Program version 2 (POP2) [Smith et al., 2010; Danabasoglu et al., 2012] is the ocean component of CESM2, the same as in CESM1 but with several advances. These include a new parameterization for mixing effects in estuaries, increased mesoscale eddy (isopycnal) diffusivities at depth, use of prognostic chlorophyll for shortwave absorption, use of salinity-dependent freezing-point together with sea-ice model, and a new Langmuir mixing parameterization in conjunction with the new wave model component [Danabasoglu et al., 2020]. POP2 operates on a mesh which is uniform in the zonal direction (1.125°) and varies significantly in the meridional direction with the finest resolution of 0.27° at the equator. In the Northern Hemisphere high latitudes, the finest and coarsest resolution is about 0.38° and 0.64° ,

respectively, at the northwestern Atlantic Ocean/northwestern Pacific Ocean. In the Southern Hemisphere, the resolution monotonically changes to 0.53° at 32°S and remains constant further south. There are 60 vertical levels with a maximum depth of 5500 m with a uniform resolution of 10 m in the upper 160 m. CESM2 uses CICE version 5.1.2 (CICE5) [Hunke et al., 2015] as its sea-ice component and uses the same horizontal grid as POP2.

CESM2 uses the Community Land Model version 5 (CLM5) [Lawrence et al., 2019] with many updates from CLM4. CLM5 improves the model's hydrological and ecological realism and enhances the representation of anthropogenic land use activities on climate and carbon cycle [Danabasoglu et al., 2020]. The River Transport Model (RTM) used in CESM1 has been replaced with the Model for Scale Adaptive River transport (MOSART) [Li et al., 2013].

3. Cloud seeding masks

Following the methodology outlined in Latham et al. [2008] and Rasch et al. [2009], to determine susceptibility to cloud seeding for each grid point, two CESM2 simulations between 2015 and 2034 under SSP2-4.5 were conducted. The first is a baseline simulation and the second assumes that MCB is deployed over all grid points over the ocean where the cloud drop number concentration of low clouds within the boundary layer (below 850 hPa) is artificially increased to $375/\text{cm}^3$. Differences in shortwave cloud forcing (SWCF) between the two simulations are the sole indicator in determining susceptibility to cloud seeding. Grid points with the strongest negative SWCF differences due to MCB are considered most susceptible to cloud seeding and all grid points over the ocean are ranked based on their susceptibility to cloud seeding. Major physical factors affecting susceptibility to cloud seeding for each grid include the amount of incoming solar radiation and the persistence of low clouds. Thus, regions in lower latitudes with persistent presence of low clouds are likely to rank higher in susceptibility to cloud seeding.

Radiative forcing under the susceptibility rankings computed from these two simulations is depicted in Figure 1. For grid points most susceptible to seeding, the radiative forcing is plotted as the blue line in Figure 1. For the top (most susceptible) 10% ocean surface, the radiative forcing is $\sim 5 \text{ W/m}^2$. For the top 20% ocean surface, the radiative forcing is only $\sim 7.6 \text{ W/m}^2$, well short of doubling from the top 10% ocean surface.

As can be seen in Figure 1, when the area extent of cloud seeding reaches 80% of the ocean surface, further area extent increase is ineffective in producing more cooling. Thus, the tail portion in the susceptibility rankings is defined as least susceptible to cloud seeding. Thus, if MCB is to be deployed over 10% of the ocean surface in the least susceptible approach, the

seeding mask will be equivalent to the difference between 80% of the ocean surface and 70% of the ocean surface most susceptible to cloud seeding.

Radiative forcing based on the least susceptible approach can reach $\sim 5 \text{ W/m}^2$ when MCB is deployed over 50% of the ocean surface, i.e., much broader than under the most susceptible approach in which deployment of MCB over 10% ocean surface is capable of achieving the same amount of cooling. The 50% ocean surface in the least susceptible approach is, by definition, equal to the top 80% ocean surface in the most susceptible approach minus the top 30% ocean surface.

The monthly seeding masks, established by the aforementioned CESM2 simulations, based on the top (most susceptible) 5% ocean surface and the tail (least susceptible) 30% ocean surface in the least susceptible approach are plotted in Figure 2. It is important to note that there is zero overlap in the two seeding masks as all grid points are ranked based on SWCF differences. As shown in red shading in Figure 2, the seeding mask under the top 5% ocean surface favors the summer hemisphere where incoming solar radiation is more abundant. Further, it also indicates that the stratocumulus regions over the eastern flank of the Pacific Ocean gyre are most susceptible to cloud seeding.

However, the seeding mask under the tail 30% ocean surface (blue shading in Figure 2) illustrates a very different pattern, and points primarily to open ocean regions, such as the Southern Ocean during the boreal summer and the North Atlantic during the boreal winter. Under this approach, deployment of MCB favors the winter hemisphere where less incoming solar radiation is available to be reflected. Further, the most favorable sites for MCB are mainly found in mid latitudes which is also a drastically different feature from the seeding mask under the top 5% ocean surface.

4. MCB experiments

Following the protocol described in Richter et al. [2022], MCB intervention is assumed to be initiated in 2035 and the simulations are performed between 2035 and 2069 in this study. The temperature target for MCB intervention is to restore the global average surface temperature between 2050 and 2069 back to the 2020-2039 level. The simulations are conducted with CESM2 under the moderate Shared Socioeconomic Pathway scenario of SSP2-4.5 for this study [O'Neill et al., 2016]. For MCB simulations, the cloud drop number concentration of low clouds within the boundary layer (below 850 hPa) over designated cloud seeding regions is artificially increased to $375/\text{cm}^3$, the lower number concentration assumed in Latham et al. [2008] which is more realistic than the higher number concentration ($1000/\text{cm}^3$). Five MCB simulations are examined in this study. Deployment of MCB is assumed to be over: 1) top 5% ocean surface (most susceptible), 2)

tail 10% ocean surface (least susceptible), 3) tail 20% ocean surface, 4) tail 30% ocean surface, and 5) tail 40% ocean surface, as listed in Table 1.

As expected, without any intervention, the global mean surface temperature in the SSP2-4.5 simulation steadily increases throughout the simulation period (black line in Figure 3a) with an average of 288.8 K between 2020 and 2039 which is the temperature target for MCB intervention. The effect of global warming under SSP2-4.5 simulated by CESM2 is illustrated in Figure 3b. In general, stronger warming is found over polar regions. Additionally, stronger warming is also present over Eastern Canada, Eastern Siberia, Northeastern and Central China. As also shown in Figure 3a (red line), the application of MCB over the top 5% ocean surface is capable of meeting the temperature target, and the average global mean surface temperature between 2050 and 2069 is 288.7 K, although it is lower than average early in the period, and over the average after year 2057. For the least susceptible approach, MCB over 10% ocean surface is insufficient to induce enough cooling, and MCB over 30% and 40% ocean surface over-cools the Earth relative to the target. The global mean surface temperature in the simulation utilizing 20% ocean surface seeding is right on the temperature target.

In order to examine the uniformity of surface temperature responses induced by MCB under various seeding strategies, we define

$$\Delta T_1 = T_{control}(2050\sim2069) - T_{control}(2020\sim2039) = \Delta T_{SSP},$$

$$\Delta T_2 = T_{MCB}(2050\sim2069) - T_{control}(2050\sim2069) = \Delta T_{MCB} + \Delta T_{SSP},$$

where ΔT_1 is the surface temperature response due to climate change (ΔT_{SSP}), and ΔT_2 is the combined effects of climate change and MCB intervention (ΔT_{MCB}), and

$$\Delta T_{MCB} = \Delta T_2 - \Delta T_1,$$

$$\gamma \cdot \Delta T_{MCB} + \Delta T_{SSP} = 0,$$

where γ is a hypothetical scaling factor for MCB intervention so the combined effects of climate change and MCB intervention sum to zero.

Even though MCB deployment over the top 5% ocean surface is capable of meeting the temperature target, its induced cooling is mainly confined to lower latitudes (Figure 3c) and this does a poor job at offsetting the pattern of warming in the SSP2-4.5 scenario. The sea surface temperature response over the Pacific Ocean resembles that of La Nina. This could pose a threat to interfere with the ENSO. In addition, there are regions where surface temperature is significantly warmer under such MCB intervention than under global warming (shown in Figure 3b), e.g. over the Northwest Pacific Ocean and the South Pacific convergence zone (SPCZ). All of these features are considered as undesirable outcomes, especially when compared with SAI

studies which have shown that SAI in general induced cooling much more evenly distributed over the globe [e.g. Tilmes et al. 2018; Richter et al. 2022].

MCB under the least susceptibility approach, however, is showing a very different surface temperature response pattern. In the four experiments (Figures. 3d, e, f, g) conducted in this study, they all show a much more uniform response compared with the high-susceptibility approach (Figure 3c). MCB over the tail 20% ocean surface is the closest in meeting the temperature target of the four experiments and the global surface temperature map (Figure 3e) indicates that it is very close to restoring the surface temperature over the globe between 2050 and 2069 to the average between 2020 and 2039. Under this MCB intervention, enough cooling is induced over the polar regions to counteract the warming effect by global warming. However, surface temperature over Eastern Canada and US, and Northeastern and Central China is slightly warmer, implying induced cooling is not sufficient to restore temperature over these regions to the 2020-2039 level. Even though MCB over the tail 30% and 40% ocean surface (Figures 3 f, g) overcools the Earth, they both show, with the hypothetical scaling, that cooling is much more evenly distributed than MCB over the top 5% ocean surface (Figure 3c). These results suggest that MCB under the least susceptible approach induces much more uniform cooling than the most susceptible approach and is perhaps a more desirable strategy of climate intervention via MCB.

In the global mean, precipitation increases in the SSP2-4.5 simulation (Fig 4a, black line). In all of the MCB simulations, global mean precipitation is reduced relative to SSP2-4.5 in varying degrees. MCB applied over the top 5% (Figure 4c) induces strong precipitation responses, e.g. decrease over the SPCZ and tropical Pacific, increase over Australia, and northward shift for the Intertropical Convergence Zone (ITCZ). The induced changes are much stronger in magnitude than the effect of global warming (Figure 4b) which indicates that the most noticeable change is enhanced precipitation over the ITCZ. However, MCB under the least susceptible approach induces much weaker regional precipitation responses (Figures 4 d, e, f, g), similar to the surface temperature response.

5. Summary and conclusion

MCB has been demonstrated in various climate models as a viable option as a solar climate intervention proposal. Even though not all the previous studies specifically assumed to deploy MCB over regions most susceptible to cloud seeding, most of them considered regions more likely to induce strong local cooling effects. While this makes sense, such an approach might lead to exerting strong regional forcing on the climate system, leading to non-uniform cooling, and triggering of unintended regional impacts to the mean climate state and its

variabilities. One common response in most MCB simulations is the triggering of a La Nina-like sea surface temperature pattern which might pose a threat to disrupt the ENSO.

In this study, we explored a different cloud seeding strategy to examine if we may be able to achieve more uniform global cooling and alleviate various undesirable outcomes frequently seen in previous MCB studies. It is hypothesized that MCB deployment over a much broader region with low susceptibility to cloud seeding might exert much weaker regional forcing on the climate system which in turn could alleviate the previously seen unintended consequences.

Our results suggest that deployment of MCB over regions with low susceptibility to cloud seeding could lead to more uniform cooling over the globe and a La Nina-like response is no longer triggered. Even though the globally-averaged radiative forcing from MCB utilizing the top 5% ocean surface and the tail 40% ocean surface is quite similar (~ -3 W/m², Figure 1), the resulting reduction in global average surface temperature is significantly different (see Figure 3a). Deployment of MCB over the tail 40% ocean surface achieves much stronger reduction in global averaged surface temperature than the top 5%. This suggests that MCB under the most susceptible approach behaves drastically differently from the least susceptible approach. Finally, it will be important to see if similar results could be reproduced in other climate models as this will allow us to gain deeper confidence for the findings in this study.

Acknowledgements

The work is based upon work supported by the NOAA ERB grant NA22OAR4310481, and the National Center for Atmospheric Research which is a major facility sponsored by the National Science Foundation under Cooperative Agreement no. 1852977. The Community Earth System Model (CESM) project is supported primarily by the National Science Foundation. Computing and data storage resources, including the Cheyenne (doi:10.5065/D6RX99HX) and Derecho (doi:10.5065/qx9a-pg09) supercomputers, were provided by the Computational and Information Systems Laboratory (CISL) at NCAR. Support for BK was provided in part by the Indiana University Environmental Resilience Institute. The Pacific Northwest National Laboratory is operated for the US Department of Energy by Battelle Memorial Institute under contract DE-AC05-76RL01830.

Open Research

Data Availability Statement

CESM tag cesm2.1.4-rc.08 was used to carry out the simulations and is available at

<https://doi.org/10.5281/zenodo.7271743> (CESM Team, 2022). CESM2 simulation output presented in this paper is available at <https://doi.org/10.5065/MRH9-B809>.

References

- Coburn, J. and Pryor, S. C.: Differential Credibility of Climate Modes in CMIP6, *J. Climate*, 34, 8145–8164, 2021.
- Danabasoglu, G., Bates, S. C., Briegleb, B. P., Jayne, S. R., Jochum, M., Large, W. G., Peacock, S., & Yeager, S. G. (2012). The CCSM4 ocean component. *Journal of Climate*, 25, 1361–1389. <https://doi.org/10.1175/JCLI-D-11-00091.1>
- Danabasoglu, G., Lamarque, J.-F., Bacmeister, J., Bailey, D. A., DuVivier, A. K., Edwards, J., et al. (2020). The Community Earth System Model Version 2 (CESM2). *Journal of Advances in Modeling Earth Systems*, 12, e2019MS001916. <https://doi.org/10.1029/2019MS001916>
- DuVivier, A. K., Holland, M. M., Kay, J. E., Tilmes, S., Gettelman, A., and Bailey, D. A.: Arctic and Antarctic sea ice mean state in the Community Earth System Model Version 2 and the influence of atmospheric chemistry, *J. Geophys. Res.-Oceans*, 125, e2019JC015934, <https://doi.org/10.1029/2019JC015934>, 2020.
- Eyring, V., Bony, S., Meehl, G. A., Senior, C. A., Stevens, B., Stouffer, R. J., & Taylor, K. E. (2016). Overview of the Coupled Model Intercomparison Project phase 6 (CMIP6) experimental design and organization. *Geoscientific Model Development*, 9, 1937–1958. <https://doi.org/10.5194/gmd-9-1937-2016>
- Friedlingstein, P., O'Sullivan, M., Jones, M. W., Andrew, R. M., Bakker, D. C. E., Hauck, J., Landschützer, P., Le Quéré, C., Luijkx, I. T., Peters, G. P., Peters, W., Pongratz, J., Schwingshackl, C., Sitch, S., Canadell, J. G., Ciais, P., Jackson, R. B., Alin, S. R., Anthoni, P., Barbero, L., Bates, N. R., Becker, M., Bellouin, N., Decharme, B., Bopp, L., Brasika, I. B. M., Cadule, P., Chamberlain, M. A., Chandra, N., Chau, T.-T.-T., Chevallier, F., Chini, L. P., Cronin, M., Dou, X., Enyo, K., Evans, W., Falk, S., Feely, R. A., Feng, L., Ford, D. J., Gasser, T., Ghattas, J., Gkritzalis, T., Grassi, G., Gregor, L., Gruber, N., Gürses, Ö., Harris, I., Hefner, M., Heinke, J., Houghton, R. A., Hurtt, G. C., Iida, Y., Ilyina, T., Jacobson, A. R., Jain, A., Jarníková, T., Jersild, A., Jiang, F., Jin, Z., Joos, F., Kato, E., Keeling, R. F., Kennedy, D., Klein Goldewijk, K., Knauer, J., Korsbakken, J. I., Körtzinger, A., Lan, X., Lefèvre, N., Li, H., Liu, J., Liu, Z., Ma, L., Marland, G., Mayot, N., McGuire, P. C., McKinley, G. A., Meyer, G., Morgan, E. J., Munro, D. R., Nakaoka, S.-I., Niwa, Y., O'Brien,

K. M., Olsen, A., Omar, A. M., Ono, T., Paulsen, M., Pierrot, D., Pocock, K., Poulter, B., Powis, C. M., Rehder, G., Resplandy, L., Robertson, E., Rödenbeck, C., Rosan, T. M., Schwinger, J., Séférian, R., Smallman, T. L., Smith, S. M., Sospedra-Alfonso, R., Sun, Q., Sutton, A. J., Sweeney, C., Takao, S., Tans, P. P., Tian, H., Tilbrook, B., Tsujino, H., Tubiello, F., van der Werf, G. R., van Ooijen, E., Wanninkhof, R., Watanabe, M., Wimart-Rousseau, C., Yang, D., Yang, X., Yuan, W., Yue, X., Zaehle, S., Zeng, J., and Zheng, B.: Global Carbon Budget 2023, *Earth Syst. Sci. Data*, 15, 5301–5369, <https://doi.org/10.5194/essd-15-5301-2023>, 2023.

Gettelman, A., & Morrison, H. (2015). Advanced two-moment bulk microphysics for global models. Part I: Off-line tests and comparison with other schemes. *Journal of Climate*, 28, 1268–1287. <https://doi.org/10.1175/JCLI-D-14-00102.1>

Golaz, J.-C., Larson, V. E., & Cotton, W. R. (2002). A PDF-based model for boundary layer clouds. Part I: Method and model description. *Journal of the Atmospheric Sciences*, 59, 3540–3551.

Haywood, J. M., Jones, A., Jones, A. C., Halloran, P., and Rasch, P. J.: Climate intervention using marine cloud brightening (MCB) compared with stratospheric aerosol injection (SAI) in the UKESM1 climate model, *Atmos. Chem. Phys.*, 23, 15305–15324, <https://doi.org/10.5194/acp-23-15305-2023>, 2023.

Hill, S., & Ming, Y. (2012). Nonlinear climate response to regional brightening of tropical marine stratocumulus: Climate response to cloud brightening. *Geophysical Research Letters*, 39(15), L15707. <https://doi.org/10.1029/2012GL052064>

Hirasawa, H., Hingmire, D., Singh, H., Rasch, P. J., & Mitra, P. (2023). Effect of regional marine cloud brightening interventions on climate tipping elements. *Geophysical Research Letters*, 50, e2023GL104314. <https://doi.org/10.1029/2023GL104314>

Hunke, E. C., Lipscomb, W. H., Turner, A. K., Jeffery, N., & Elliott, S. (2015). CICE: The Los Alamos Sea Ice Model. Documentation and Software User's Manual. Version 5.1. *T-3 Fluid Dynamics Group*, Los Alamos National Laboratory, Tech. Rep. LA-CC-06-012.

Jones, A., Haywood, J., & Boucher, O. (2009). Climate impacts of geoengineering marine stratocumulus clouds. *Journal of Geophysical Research*, 114(D10), 2008JD011450. <https://doi.org/10.1029/2008JD011450>

Larson, V. E., (2017). CLUBB-SILHS: A parameterization of subgrid variability in the atmosphere. arXiv:1711.03675v2 [physics.ao-ph].

Latham, J., Rasch, P., Chen, C.-C., Kettles, L., Gadian, A., Gettelman, A., Morrison, H., Bower, K., and Choulaton, T.: Global Temperature Stabilization via Controlled Albedo

Enhancement of Low-Level Maritime Clouds, *Philos. T. R. Soc. A*, 366, 1882, 3969–3987, <https://doi.org/10.1098/rsta.2008.0137>, 2008.

Lawrence, D. M., Fisher, R. A., Koven, C. D., Oleson, K. W., Swenson, S. C., Bonan, G., Collier, N., Ghimire, B., van Kampenhout, L., Kennedy, D., Kluzek, E., Lawrence, P. J., Li, F., Li, H., Lombardozzi, D., Riley, W. J., Sacks, W. J., Shi, M., Vertenstein, M., Wieder, W. R., Xu, C., Ali, A. A., Badger, A. M., Bisht, G., Brunke, M. A., Burns, S. P., Buzan, J., Clark, M., Craig, A., Dahlin, K., Drewniak, B., Fisher, J. B., Flanner, M., Fox, A. M., Gentine, P., Hoffman, F., Keppel-Aleks, G., Knox, R., Kumar, S., Lenaerts, J., Leung, L. R., Lipscomb, W. H., Lu, Y., Pandey, A., Pelletier, J. D., Perket, J., Randerson, J. T., Ricciuto, D. M., Sanderson, B. M., Slater, A., Subin, Z. M., Tang, J., Thomas, R. Q., Val Martin, M., & Zeng, X. (2019). The Community Land Model Version 5: Description of new features, benchmarking, and impact of forcing uncertainty. *Journal of Advances in Modeling Earth Systems*, 11, 4245–4287. <https://doi.org/10.1029/2018MS001583>

Li, F., Levis, S., & Ward, D. S. (2013). Quantifying the role of fire in the Earth system—Part 1: Improved global fire modeling in the Community Earth System Model (CESM1). *Biogeosciences*, 10, 2293–2314. <https://doi.org/10.5194/bg-10-2293-2013>

MacMartin, D. G., Wang, W., Kravitz, B., Tilmes, S., Richter, J. H., and Mills, M. J.: Timescale for detecting the climate response to stratospheric aerosol geoengineering, *J. Geophys. Res.-Atmos.*, 124, 1233–1247, <https://doi.org/10.1029/2018JD028906>, 2019.

MacMartin, D. G., Kravitz, B., Tilmes, S., Richter, J. H., Mills, M. J., Lamarque, J.-F., Tribbia, J. J., and Vitt, F.: The climate response to stratospheric aerosol geoengineering can be tailored using multiple injection locations, *J. Geophys. Res.-Atmos.*, 122, 12574–12590, <https://doi.org/10.1002/2017JD026868>, 2017.

MacMartin, D. G., Visoni, D., Kravitz, B., Richter, J. H., Felgenhauer, T., Lee, W., Morrow, D., and Sugiyama, M.: Scenarios for modeling solar geoengineering, *P. Natl. Acad. Sci. USA*, 119, e2202230119, <https://doi.org/10.1073/pnas.2202230119>, 2022.

O'Neill, B. C., Tebaldi, C., van Vuuren, D. P., Eyring, V., Friedlingstein, P., Hurtt, G., Knutti, R., Kriegler, E., Lamarque, J.-F., Lowe, J., Meehl, G. A., Moss, R., Riahi, K., and Sanderson, B. M.: The Scenario Model Intercomparison Project (ScenarioMIP) for CMIP6, *Geosci. Model Dev.*, 9, 3461–3482, <https://doi.org/10.5194/gmd-9-3461-2016>, 2016.

Rasch, P. J., Latham, J., and Chen, C.-C.: Geoengineering by Cloud Seeding: Influence on Sea Ice and Climate System, *Environ. Res. Lett.*, 4, 045112, <https://doi.org/10.1088/1748-9326/4/4/045112>, 2009.

- Richter, J. H., Vioni, D., MacMartin, D. G., Bailey, D. A., Rosenbloom, N., Dobbins, B., Lee, W. R.,
Tye, M., and Lamarque, J.-F.: Assessing Responses and Impacts of Solar climate intervention on
the Earth system with stratospheric aerosol injection (ARISE-SAI): protocol and initial results
from the first simulations, *Geosci. Model Dev.*, 15, 8221–8243, <https://doi.org/10.5194/gmd-15-8221-2022>, 2022.
- Simpson, I. R., Bacmeister, J., Neale, R. B., Hannay, C., Gettelman, A., Garcia, R. R., et al.
(2020). An evaluation of the large-scale atmospheric circulation and its variability in
CESM2 and other CMIP models. *Journal of Geophysical Research: Atmospheres*, 125,
e2020JD032835. <https://doi.org/10.1029/2020JD032835>
- Smith, R., P. Jones, B. Briegleb, F. Bryan, G. Danabasoglu, J. Dennis, J. Dukowicz, C. Eden, B.
Fox-Kemper, P. Gent, M. Hecht, S. Jayne, M. Jochum, W. Large, K. Lindsay, M. Maltrud,
N. Norton, S. Peacock, M. Vertenstein, & S. Yeager (2010). The Parallel Ocean Program
(POP) reference manual, Ocean component of the Community Climate System Model
(CCSM), LANL Tech. Report, LAUR-10-01853, 141 pp.
- Tilmes, S., Richter, J. H., Kravitz, B., MacMartin, D. G., Mills, M. J., Simpson, I. R., Glanville, A. S.,
Fasullo, J. T., Phillips, A. S., Lamarque, J., Tribbia, J., Edwards, J., Mickelson, S., and Ghosh, S.:
CESM1(WACCM) Stratospheric Aerosol Geoengineering Large Ensemble Project, *B. Am.
Meteorol. Soc.*, 99, 2361–2371, 2018.
- Zhang, G. J., & McFarlane, N. A. (1995). Sensitivity of climate simulations to the
parameterization of cumulus convection in the Canadian climate center general-circulation
model. *Atmosphere-Ocean*, 33(3), 407–446

	Ts (K) 2020-2039	Ts (K) 2050-2069	MCB scaling factor	pr (mm/day) 2020-2039	pr (mm/day) 2050-2069
control	288.8	289.8		2.98	3.05
5% most susceptible		288.7	0.88		2.96
10% least susceptible		289.4	2.34		3.02
20% least susceptible		288.8	0.98		2.97
30% least susceptible		288.3	0.65		2.93
40% least susceptible		287.6	0.44		2.88

Table 1: Global average surface temperature and precipitation under the control and 5 MCB simulations examined in this study, and the hypothetical MCB scaling factor to allow MCB interventions to restore surface temperature between 2050 and 2069 to the 2020-2039 level.

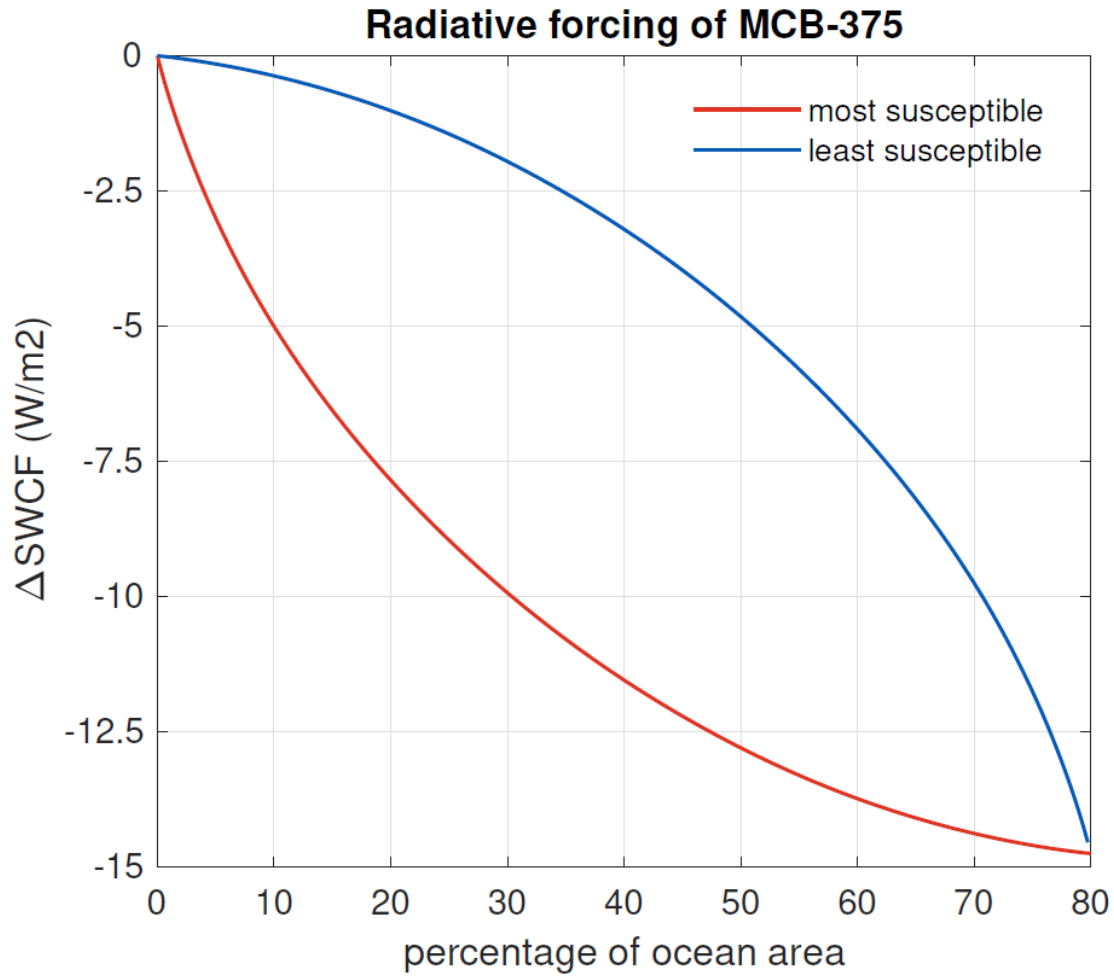


Figure 1: Radiative forcing based on susceptibility to cloud seeding. The blue line represents the most susceptible approach and the red line represents the least susceptible approach. For the least susceptible approach, 10% ocean surface seeding is taken as the difference between the top 80% most susceptible regions and the top 70% most susceptible regions.

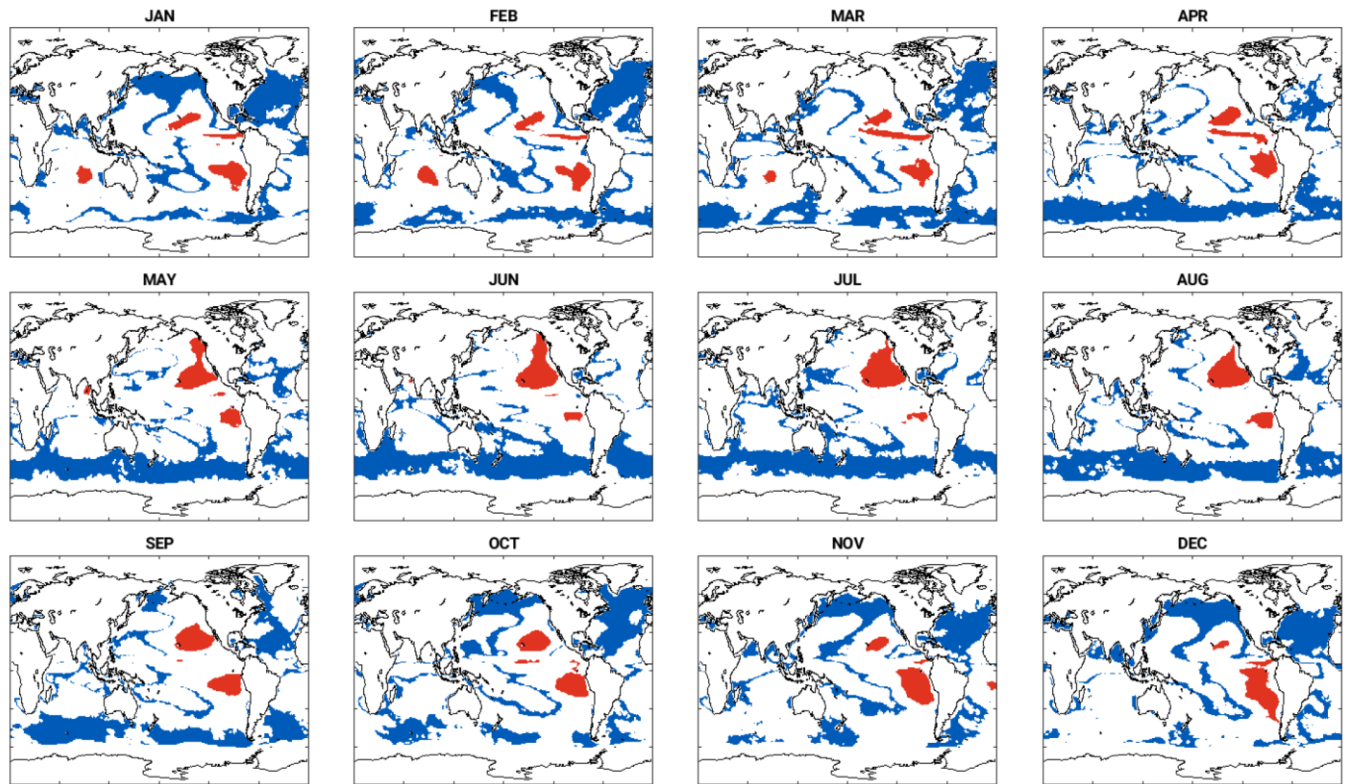


Figure 2: Monthly seeding masks: red shading represents the top 5% ocean surface most susceptible to seeding, and blue shading represents the tail 30% ocean surface least susceptible to seeding.

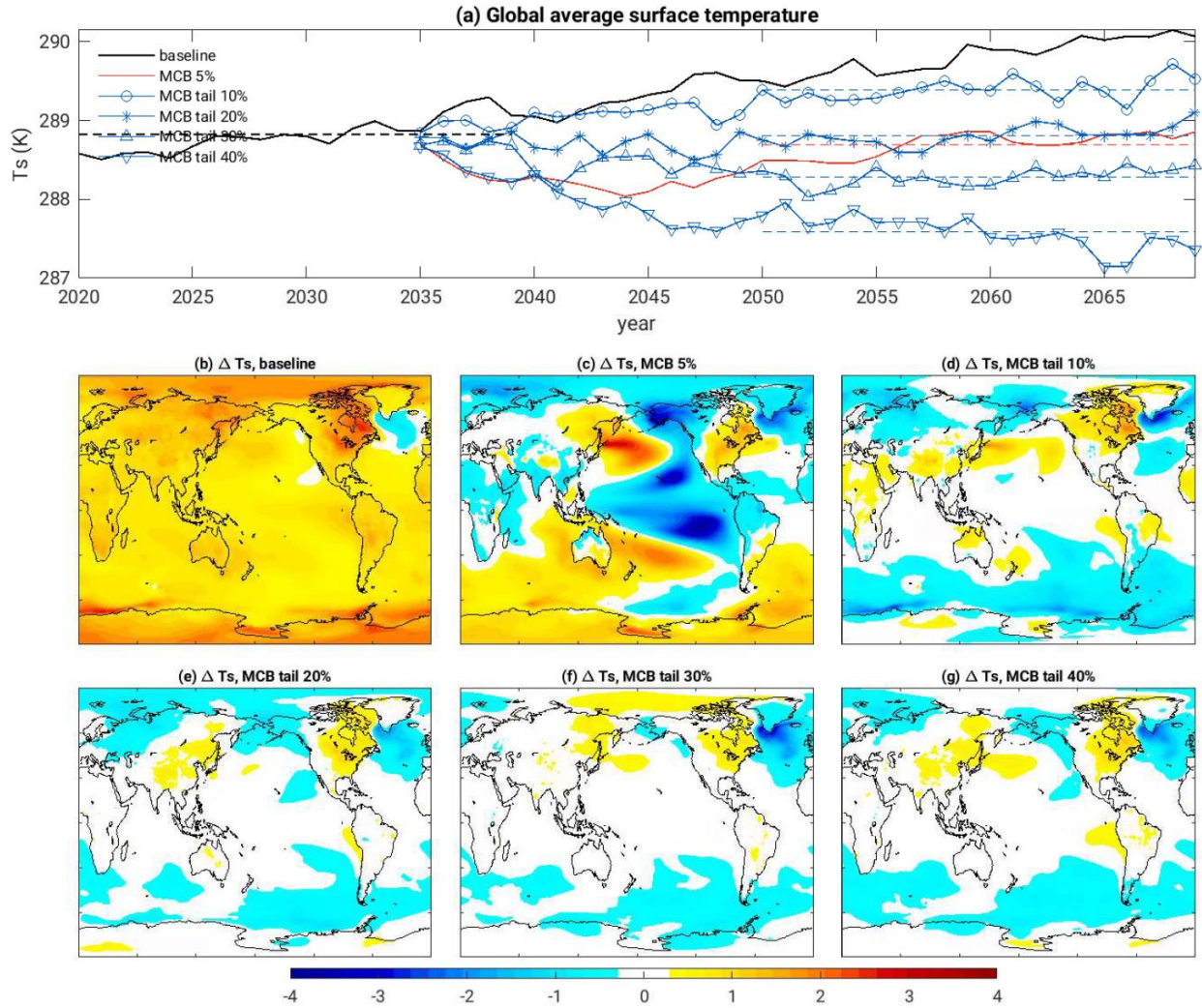


Figure 3: Global average surface temperature trend (a) and global maps of adjusted surface temperature differences of averages between 2050 and 2069 and the baseline average between 2020 and 2039 (b)-(g). A baseline CESM2 simulation is compared against MCB over 5% ocean surface most susceptible to seeding and 10%, 20%, 30% and 40% ocean surface least susceptible to seeding. The adjustment made in the difference is by applying a scaling factor on the MCB response as listed in Table 1. In (a), black dashed line represents the average between 2020 and 2039 as the MCB intervention temperature target, other dashed lines represent the averages between 2050 and 2069.

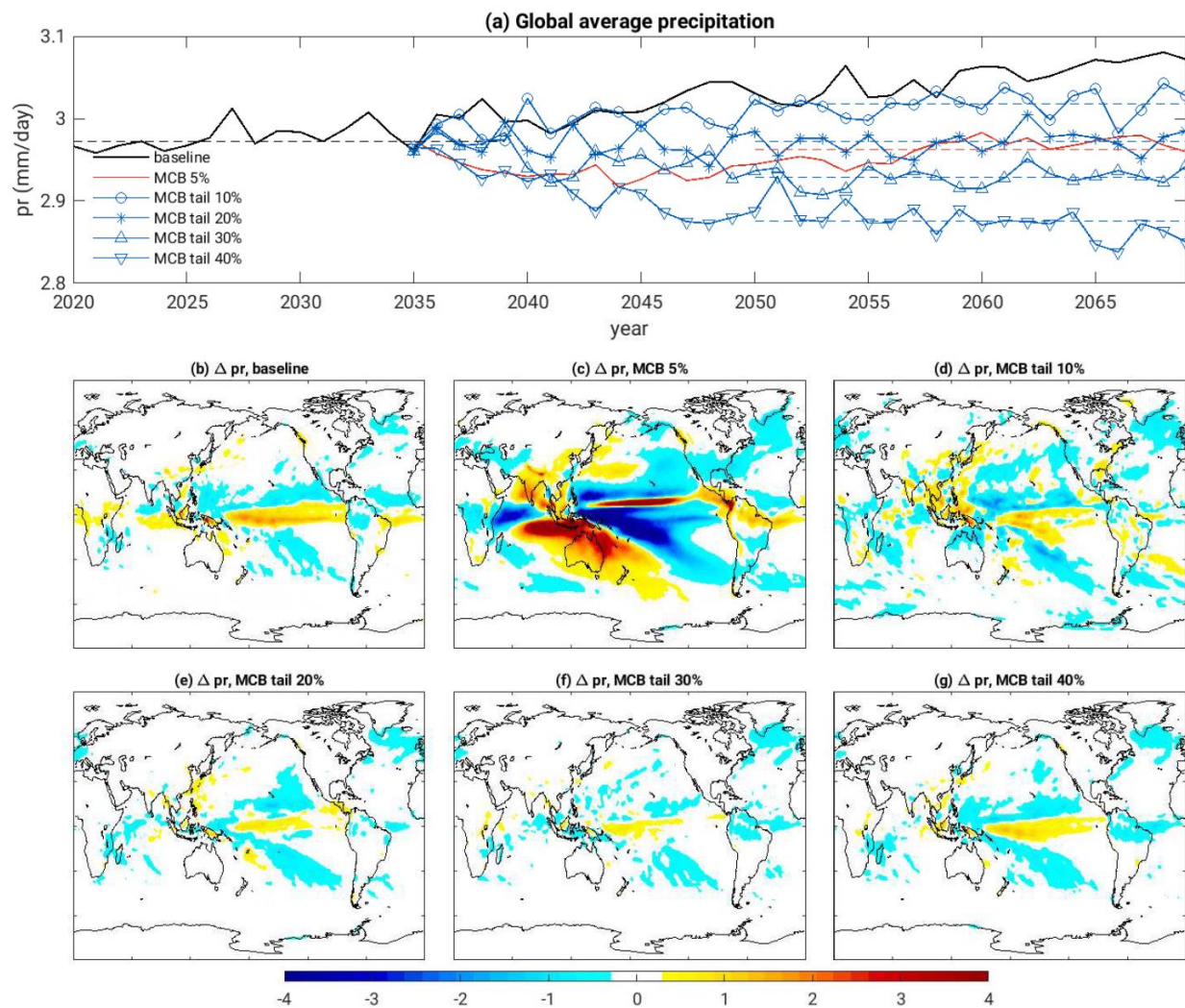


Figure 4: Similar as Fig. 3 but for precipitation rate.